at room temperature. The blots were then incubated with horseradish peroxidase-conjugated goat anti-rabbit IgG (0.08 μg/ml, Santa Cruz Biotechnology). The antibody was visualized using an enhanced chemiluminescence method (ECL; Amersham Biosciences, Piscataway, NJ, USA). The integrated density of the eNOS bands was normalized by actin band density (relative density) (NIH Image).

Regional blood flow and infarct size

To confirm infarct size reduction by edaravone in relation to the effect of collateral flow, regional MBF was assessed by non-radioactive microspheres (Sekisui Plastic Co., Ltd., Tokyo), as previously described (17). Briefly, 1 ml of the microsphere suspension (2 to 4 $\times$ 10^6 spheres) was injected into the left atrium 85 min after the onset of coronary occlusion. MBF was measured by assessing X-ray spectra of the fluorescent stable heavy elements using a wavelength-dispersive spectrometer (model PW 1480; Philips Co., Ltd., Eindhoven, the Netherlands). Myocardial collateral flow (ml/min per gram) was calculated using the following formula: tissue flow-rate = tissue counts $\times$ (reference flow / reference counts).

Myocardial short-axis slices (5-mm-thickness) of the left ventricle were made and incubated in 1% 2,3,5-triphenyltetrazoliumchloride solution (Sigma, Tokyo) for 10 min to identify the infarct area. Infarct size was expressed as a percentage of the infarct area relative to the area of risk (18).

Statistical analysis

Data are expressed as the mean $\pm$ S.E.M. The vascular response was analyzed by one-way analysis of variance followed by a Scheffe's post-hoc test for multiple comparisons (Figs. 1C, 2, 3, and 4). Regression analysis was applied in Fig. 5. Statistical significance was defined as $P<0.05$.

Results

Hemodynamics

Hemodynamic data are shown in Table 1. Mean arterial pressure and heart rate during administration of acetylcholine and papaverine were not statistically different as compared to their respective baseline. Hemodynamic variables at baseline did not significantly change before and after I/R nor after edaravone administration.

Endothelium-dependent vasodilation

We assessed the diameter changes of 22 coronary microvessels under acetylcholine (1 μg/kg, i.c.) in each group. The diameter changes of small artery and arteriole in each group are depicted in Fig. 1, A and B. Under control conditions (without edaravone), I/R strikingly impaired endothelium-dependent vasodilation at 60 min after I/R. Meanwhile, edaravone administration augmented the response in coronary microvessels of both sizes. Preservation of vasodilation under acetylcholine was more prominent in the small artery than the arteriole. Coronary flow in the presence of acetylcholine was improved after I/R in the edaravone-adminstered group compared with that in the controls (without edaravone) (Fig. 1C).

ROS intensity in coronary microvessels

Fifteen coronary microvessels (<300 μm) were assessed from both the LAD and LCX areas in both groups (Fig. 2). ROS fluorescent intensity at 60 min after I/R in the microvessels from the LAD area in the control group was higher than in the LCX area ($P<0.01$). Meanwhile, ROS intensity in the microvessels from the LAD area of the edaravone group was significantly lower than that in the control group ($P<0.01$).

Intensity of NO in coronary microvessels

Fluorescent intensity of NO in the endothelial layer was assessed semi-quantitatively in 15 microvessels from the LAD or LCX areas in both groups 60 min after

Table 1. Hemodynamics data before and after ischemia/reperfusion

	Before I/R			After I/R		
	Baseline	Acetylcholine	Papaverine	Baseline	Acetylcholine	Papaverine
Mean blood pressure (mmHg)						
Control	91 $\pm$ 4	90 $\pm$ 6	91 $\pm$ 4	89 $\pm$ 4	89 $\pm$ 5	87 $\pm$ 5
Edaravone	92 $\pm$ 2	91 $\pm$ 4	90 $\pm$ 3	93 $\pm$ 3	91 $\pm$ 5	90 $\pm$ 4
Heart rate (beats/min)						
Control	123 $\pm$ 5	125 $\pm$ 3	126 $\pm$ 4	120 $\pm$ 4	122 $\pm$ 5	120 $\pm$ 5
Edaravone	124 $\pm$ 4	126 $\pm$ 6	123 $\pm$ 5	123 $\pm$ 4	121 $\pm$ 5	120 $\pm$ 4

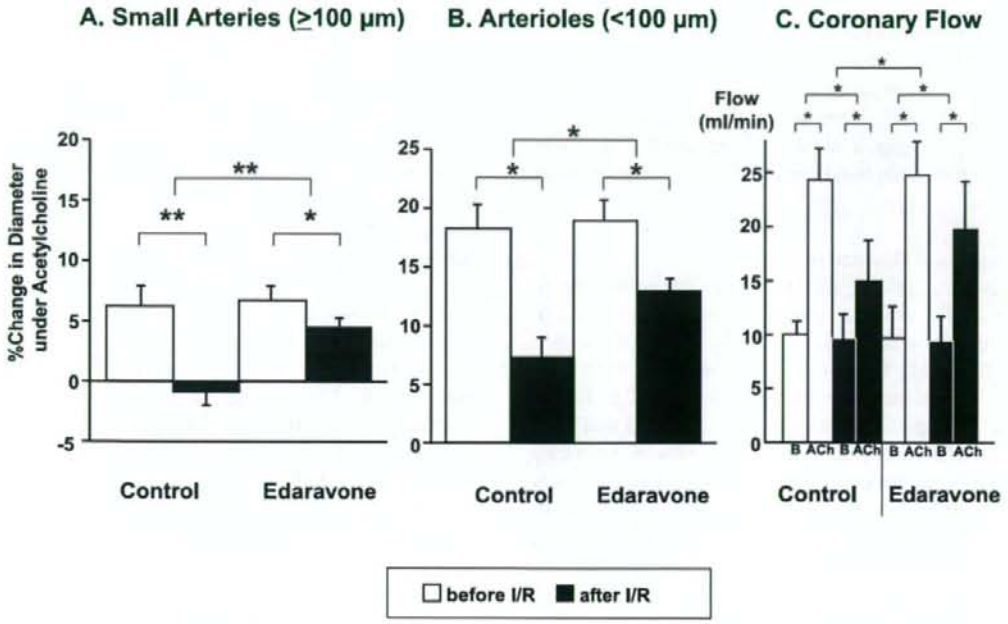

Fig. 1. Endothelium-dependent vasodilation in coronary microvessels in vivo. Edaravone administration augmented the vasodilation of small arteries (A) and arterioles (B) and improved coronary flow (C) under acetylcholine after I/R. Number of small arteries and arterioles assessed were 10 and 12, respectively. *P<0.05, **P<0.01. B = baseline, ACh = acetylcholine.

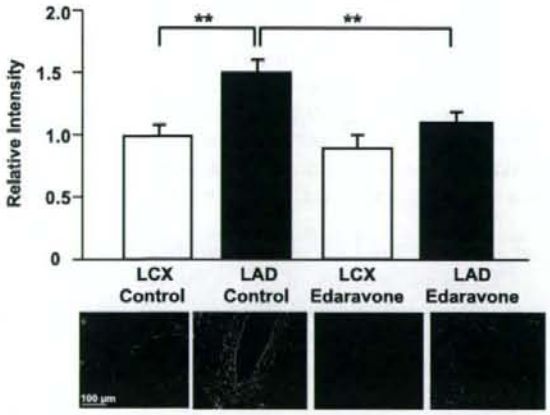

Fig. 2. In situ detection of ROS in coronary microvessels after I/R. The fluorescent intensity of ROS in microvessels from each area is shown (n = 15, in each area) with their representative DHE-fluorescence image of ROS in the vessels. **P<0.01.

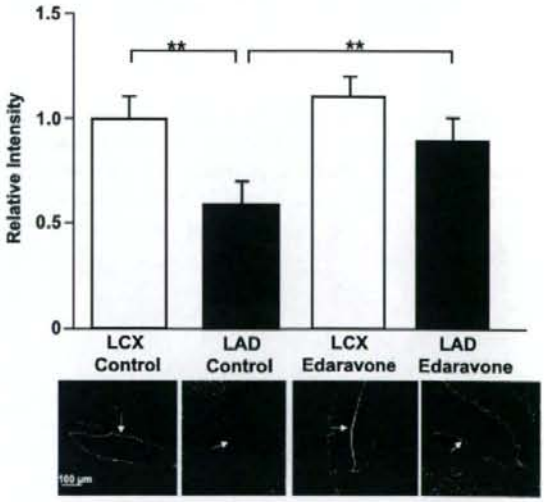

Fig. 3. In situ detection of NO in coronary microvessels after I/R. Fluorescent intensity of NO in microvessels from each area is shown (n = 15, in each area) with their representative DAF2-DA fluorescence image of NO in the endothelial layer (white arrow). **P<0.01.

I/R (Fig. 3). In the LAD area of the control group (without edaravone), I/R reduced the microvascular NO intensity level as compared to the LCX area (P<0.01). Administration of edaravone significantly preserved NO

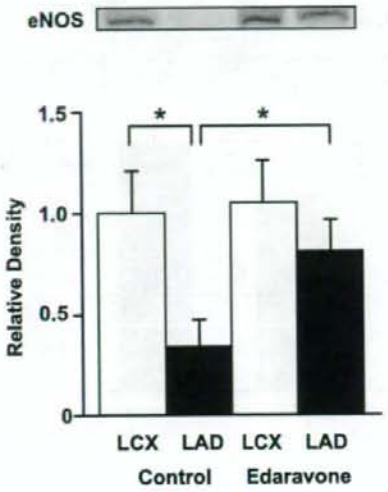

Fig. 4. eNOS protein immunoblotting after I/R. Edaravone administration augmented myocardial eNOS expression after I/R in the ischemic area. *$P<0.05$.

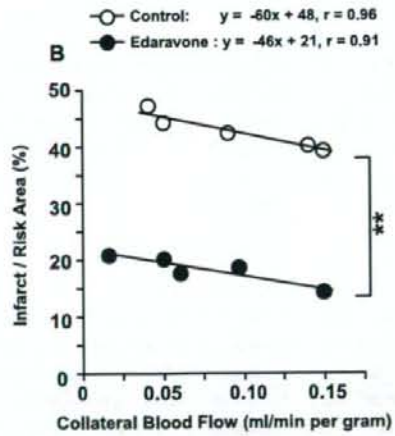

Fig. 5. Correlation of regional collateral flow and infarct size in the control and edaravone groups. **$P<0.01$.

fluorescent intensity in microvessels of LAD relative to the control group ($P<0.01$).

Myocardial eNOS expression

Myocardial eNOS protein expression in the LAD distribution after I/R was significantly decreased relative to the LCX area in the control group (without edaravone, $P<0.05$, Fig. 4). Edaravone augmented eNOS protein expression in the LAD area ($P<0.05$ *vs* controls).

Collateral flow and infarct size

There were linear negative correlations between regional collateral MBF and infarct size in the control ($y=-60X+48$, $r=0.96$, $P<0.001$) and edaravone ($y=-46X+21$, $r=0.91$, $P<0.001$) groups, which were significantly different between the 2 groups ($P<0.01$, Fig. 5). This finding indicated that the protective effect of edaravone was independent of collateral flow.

Endothelium-independent vasodilation

Endothelium-independent vasodilation with papaverine (1 mg, i.c.) was comparable under all conditions (Fig. 6). Administration of edaravone did not result in any significant diameter changes in small arteries and arterioles under papaverine after I/R.

Discussion

The present study revealed that edaravone preserves endothelium-dependent vasodilation in coronary small arteries and arterioles after I/R injury on the beating canine heart in vivo by reducing ROS and thereby augmenting NO availability in the microvessels. To our knowledge, the present study is the first to report that edaravone exerts protective effects on the coronary microvascular endothelial function after I/R on the beating heart in vivo.

Scavenging ROS by edaravone during ischemia/reperfusion

Generation of ROS during I/R has been shown through several mechanisms such as the xanthine oxidase, mitochondrial electron transport chain, and NADPH oxidase pathways (10). In the present study, we revealed that edaravone scavenged ROS generated in coronary microvessels during I/R (Fig. 2). Previous studies have shown other beneficial effects of edaravone such as inhibition of the production of superoxide anion on the infarct rim (14), suppression of lipid peroxidation products (19), and reduction in inflammatory changes (20).

The burst of vascular ROS production following I/R led to endothelial dysfunction, which may have occurred as a result of hypoxic injury, manifested by endothelial cell swelling that results in the no reflow phenomenon within the first minutes of reperfusion (21). The ROS may also rapidly react with NO to form a toxic peroxynitric radical (i.e., $ONOO^-$) that further increases free radical accumulation resulting in endothelial injury (9). If the ischemia lasts for hours, structural changes such as edematous mitochondria in endothelial and smooth muscle cells, microvili formation on the surface of endothelial cells, and increased pinocytic activity and

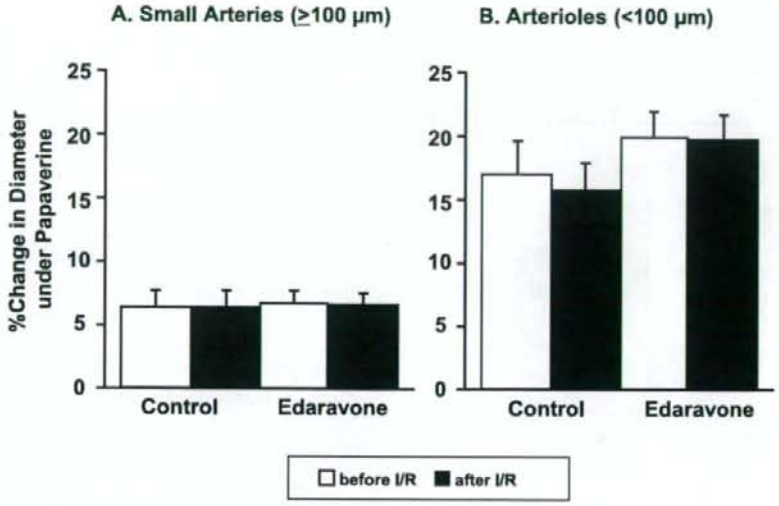

Fig. 6. Endothelium-independent vasodilation in coronary microvessels before and after I/R. The vasodilation is comparable under all conditions.

disturbed tight junctions between endothelial cells may be found by electronmicroscopical examination (21). With edaravone administration, NO bioavailability in the ischemic area endothelial layer of microvessels was significantly augmented (Fig. 3). In other settings, edaravone has also been shown to improve peripheral flow-mediated dilatation in smokers (22). Taken together, free radical scavenging by edaravone in the vessels results in preservation of NO availability and thereby maintains endothelial function, which is crucial for the cardiovascular system in both the short-term and long-term.

Edaravone preserves nitric oxide and eNOS

We have previously shown that endothelium-dependent vasodilation by acetylcholine would increase NO release in coronary circulation, indicating the central role of NO (23). However, the regulation of coronary vascular tone may be mediated, not only by NO, but also by the endothelium derived hyperpolarizing factor (EDHF) and adenosine (24). Yada et al. have demonstrated that endogeneous H_2O_2, an EDHF, and rho-kinase inhibition mediated coronary vasodilation to a greater extent in arterioles than in small arteries (7, 8, 24). In the present study, preservation of endothelium-dependent vasodilation by edaravone was noted to a greater extent in the small arteries (Fig. 1). These facts revealed various mechanisms and 'site-specific' action of different drugs or agents in the coronary circulation. These also indicated a predominant role of NO in small arteries, as opposed to arterioles. Taken together, the protective effects of NO and EDHF in coronary microvessels during I/R may occur in a compensatory manner.

Most of the NO production in the normal heart is accounted for by the presence of nitric-oxide synthase (eNOS) in the coronary endothelium and myocardium. Impaired NO synthesis from eNOS is a mechanism of endothelial dysfunction in the post-ischemic heart. The present study demonstrated reduced eNOS protein expression in the ischemic myocardium after I/R, whereas edaravone administration preserved the expression (Fig. 4). Previous studies from our institution have also demonstrated a decrease in eNOS protein expression in ischemic myocardium following I/R (7, 8). An in vitro study in HUVEC has shown that edaravone may increase eNOS expression via the inhibition of LDL oxidation (25). Thus, the burst of ROS generation during I/R may cause cell injury that results in reduced eNOS production, and edaravone administration preserves the eNOS expression.

Myocardial protection by edaravone

The present study confirmed the protective effect of edaravone on the myocardial cell (13) and revealed that the cardioprotective role of edaravone during I/R was irrespective of transmural collateral flow to the ischemic area (Fig. 5). It has been hypothesized that maintenance of endothelium-dependent dilation of coronary microvessels could enhance reperfusion damage and reduces the amount of tissue necrosis (26). Thus, preservation of microvascular endothelial function

by edaravone probably contributed to the improvement in myocardial perfusion, thereby facilitating myocardial tissue preservation after I/R.

In the present study, we administered edaravone prior to coronary occlusion because ROS generation may occur during occlusion and after reperfusion. Wu et al. have shown a protective effect of edaravone on the myocardium when it was administered during coronary occlusion or after reperfusion (27). Thus, we presumed that preservation of endothelial function by edaravone may also be observed if it is administered during occlusion or after reperfusion. Nevertheless, further study is needed to confirm these issues.

Conclusions

In conclusion, edaravone exerts beneficial protective effects on coronary microvessels by preserving endothelial function after I/R in vivo. These effects are attributed to the ROS scavenging properties of edaravone and involves an NO-mediated mechanism.

Acknowledgments

This work was supported in part by a grant (No 16300164) from the Japanese Ministry of Education, Science, Sports, Culture, and Technology and a grant from the program for promotion of fundamental studies in health sciences of the Organization for Pharmaceutical Safety and Research in Japan.

References

1 Chilian WM, Kuo L, DeFily DV, Jones CJ, Davis MJ. Endothelial regulation of coronary microvascular tone under physiological and pathophysiological conditions. Eur Heart J. 1993;1 Suppl I:55–59.

2 Kuo L, Davis MJ, Chilian WM. Endothelium-dependent, flow-induced dilation of isolated coronary arterioles. Am J Physiol. 1990;259:1063–1170.

3 Suwaidi JA, Hamasaki S, Higano ST, Nishimura RA, Holmes DR, Lerman A. Long-term follow-up of patients with mild coronary artery disease and endothelial dysfunction. Circulation. 2000;101:948–954.

4 Schächinger V, Britten B, Zeiher AM. Prognostic impact of coronary vasodilator dysfunction on adverse long-term outcome of coronary heart disease. Circulation. 2000;101:1899–1906.

5 Targonski PV, Bonetti PO, Pumper GM, Higano ST, Holmes DR, Lerman A. Coronary endothelial dysfunction is associated with an increased risk of cerebrovascular events. Circulation. 2003;107:2805–2809.

6 Matsumura K, Jeremy RW, Schaper J. Progression of myocardial necrosis during reperfusion of ischemic myocardium. Circulation. 1998;97:795–804.

7 Yada T, Shimokawa H, Hiramatsu O, Kajita T, Shigeto F, Tanaka E, et al. Beneficial effect of hydroxyfasudil, a specific Rho-kinase inhibitor, on ischemia/reperfusion injury in canine coronary microcirculation in vivo. J Am Coll Cardiol. 2005;45:599–607.

8 Yada T, Shimokawa H, Hiramatsu O, Haruna Y, Morita Y, Kashihara N, et al. Cardioprotective role of endogenous hydrogen peroxide during ischemia-reperfusion injury in canine coronary microcirculation in vivo. Am J Physiol Heart Circ Physiol. 2006;291:H1138–1146.

9 Bolli R, Jeroudi MO, Patel BS, DuBose CM, Lai EK, Roberts R, et al. Direct evidence that oxygen-derived free radicals contribute to postischemic myocardial dysfunction in the intact dog. Proc Natl Acad Sci U S A. 1989;86:4695–4699.

10 Zweier JL, Talukder MA. The role of oxidants and free radicals in reperfusion injury. Cardiovasc Res. 2006;70:181–190.

11 Becker LB, vanden Hoek TL, Shao ZH, Li CQ, Schumacker PT. Generation of superoxide in cardiomyocytes during ischemia before reperfusion. Am J Physiol. 1999;277:H2240–H2246.

12 Kevin LG, Camara AK, Riess ML, Novalija E, Stowe DF. Ischemic preconditioning alters real-time measure of O_2 radicals in intact hearts with ischemia and reperfusion. Am J Physiol Heart Circ Physiol. 2003;284:H566–H574.

13 Yamawaki M, Sasaki N, Shimoyama M, Miake J, Ogino K, Igawa O, et al. Protective effect of edaravone against hypoxia-reoxygenation injury in rabbit cardiomyocytes. Br J Pharmacol. 2004;142:618–626.

14 Shichinohe H, Kuroda S, Yasuda H, Ishikawa T, Iwai M, Horiuchi M. Neuroprotective effects of the free radical scavenger edaravone (MCI-186) in mice permanent focal brain ischemia. Brain Res. 2004;1029:200–206.

15 Yada T, Hiramatsu O, Kimura A, Goto M, Ogasawara Y, Tsujioka K. In vivo observation of subendocardial microvessels of the beating porcine heart using a needle-probe video-microscope with a CCD camera. Circ Res. 1993;72:939–946.

16 Satoh M, Fujimoto S, Haruna Y, Arakawa S, Horike H, Komai N, et al. NAD(P)H oxidase and uncoupled nitric oxide synthase are major sources of glomerular superoxide in rats with experimental diabetic nephropathy. Am J Physiol Renal Physiol. 2005;288:F1144–F1152.

17 Mori H, Haruyama S, Shinozaki Y, Okino H, Iida A, Takanashi R, et al. New nonradioactive microspheres and more sensitive X-ray fluorescence to measure regional blood flow. Am J Physiol Heart Circ Physiol.1992;263:H1946–H1957.

18 Ogita H, Node K, Asanuma H, Sanada S, Takashima S, Asakura M. Amelioration of ischemia- and reperfusion-induced myocardial injury by the selective estrogen receptor modulator, raloxifene, in the canine heart. J Am Coll Cardiol. 2002;40:998–1005.

19 Zhang N, Komine-Kobayashi M, Tanaka R, Liu M, Mizuno Y, Urabe T. Edaravone reduces early accumulation of oxidative products and sequential inflammatory responses after transient focal ischemia in mice brain. Stroke. 2005;36:2220–2225.

20 Nimata M, Okabe TA, Hattori M, Yuan Z, Shioji K, Kishimoto C. MCI-186 (edaravone), a novel free radical scavenger, protects against acute autoimmune myocarditis in rats. Am J Physiol Heart Circ Physiol. 2005;289:H2514–H2518.

21 Szocs K. Endothelial dysfunction and reactive oxygen species production in ischemia/reperfusion and nitrate tolerance. Gen Physiol Biophys. 2004;23:265–269.

22 Jitsuiki D, Higashi Y, Goto C, Kimura M, Noma K, Hara K, et al. Effect of edaravone, a novel free radical scavenger, on

endothelium-dependent vasodilation in smokers. Am J Cardiol. 2004;94:1070–10703.

23 Neishi Y, Mochizuki S, Miyasaka T, Kawamoto T, Kume T, Sukmawan R, et al. Evaluation of bioavailability of nitric oxide in coronary circulation by direct measurement of plasma nitric oxide concentration. Proc Natl Acd Sci U S A. 2005;102:11456–11461.

24 Yada T, Shimokawa H, Hiramatsu O, Kajita T, Shigeto F, Goto M, et al. Hydrogen peroxide, an endogenous endothelium-derived hyperpolarizing factor, plays an important role in coronary autoregulation in vivo. Circulation. 2003;107:1040–1045.

25 Yoshida H, Sasaki K, Namiki Y, Sato N, Tada N. Edaravone, a novel radical scavenger, inhibits oxidative modification of low-density lipoprotein (LDL) and reverses oxidized LDL-mediated reduction in the expression of endothelial nitric oxide synthase. Atherosclerosis. 2005;179:97–102.

26 DeFily DV, Chilian WM. Preconditioning protects coronary arteriolar endothelium from ischemia-reperfusion injury. Am J Physiol. 1993;265:H700–H706.

27 Wu TW, Zeng LH, Wu J, Fung KP. Myocardial protection of MCI-186 in rabbit ischemia-reperfusion. Life Sci. 2002;71: 2249–2255.

FEBS Letters 581 (2007) 5859–5864

Crystal structure of RVV-X: An example of evolutionary gain of specificity by ADAM proteinases

Soichi Takeda*, Tomoko Igarashi, Hidezo Mori

Department of Cardiac Physiology, National Cardiovascular Center Research Institute, 5-7-1 Fujishiro-dai, Suita, Osaka 565-8565, Japan

Received 2 November 2007; revised 21 November 2007; accepted 21 November 2007

Available online 3 December 2007

Edited by Hans Eklund

Abstract **Russell's viper venom factor X activator (RVV-X) is a heterotrimeric metalloproteinase with a mammalian ADAM-like heavy chain and two lectin-like light chains. The crystal structure of RVV-X has been determined at 2.9 Å resolution and shows a hook-spanner-wrench-like architecture, in which the metalloproteinase/disintegrin region constitutes a hook, and the lectin-like domains constitute a handle. A 6.5 nm separation between the catalytic site and a putative exosite suggests a docking model for factor X. The structure provides a typical example of the molecular evolution of multi-subunit proteins and insights into the molecular basis of target recognition and proteolysis by ADAM/adamalysin/reprolysin proteinases.**

Keywords: Metalloproteinase; Disintegrin; ADAM; Factor X activator; Snake venom; Reprolysin

1. Introduction

Blood coagulation factor X is a serine proteinase and is one of the key components of the hemostatic system [1]. In circulation, factor X exists as a zymogen and is converted to an active form, factor Xa, by cleavage of a single peptide bond between Arg194 and Ile195. This removes the heavily glycosylated first 52 amino terminal residues (AP: active peptide) of the heavy chain, resulting in exposure of the active site. Factor Xa in turn converts prothrombin to thrombin, which ultimately leads to formation of hemostatic plugs.

Venom from Russell's viper, *Daboia russelli*, has been recognized for its potent coagulation activity. Russell's viper venom factor X activator (RVV-X) is a well-characterized metalloproteinase which specifically activates factor X by cleaving the same Arg-Ile bond in factor X that is cleaved by factors IXa and VIIa during physiological coagulation [2,3]. RVV-X belongs to the P-IV class of snake venom metalloproteinases [4] and consists of a heavy chain of 57,600 Da and two light chains of 19,400 and 16,400 Da, linked by disulfide bonds [2,5,6]. The 427-residue heavy chain contains the metalloproteinase (M)/disintegrin (D)/cysteine-rich (C) domains [4,7] that are shared by the (ADAM) (a disintegrin and metalloproteinase)/adamalysin/reprolysin family proteins. ADAMs are membrane-anchored glycoproteins that can proteolytically release cell-surface-protein ectodomains, including cell adhesion molecules, growth factor precursors and their receptors, and have been associated with numerous diseases including rheumatoid arthritis, Alzheimer's disease, heart disease, and cancer [8,9]. The light chains of RVV-X share amino acid sequence homology with mammalian C-type (Ca^{2+}-dependent) lectins and C-type lectin-like proteins (CLPs) isolated from various snake venoms [7,10]. RVV-X is one of the best examples of an exogenous activators used in coagulation research and has also been frequently used in diagnostic applications [2]. However, the molecular mechanism by which RVV-X recognizes and cleaves factor X is poorly understood, primarily due to the lack of three-dimensional structural information.

We recently determined the three-dimensional structure of the metalloproteinase/disintegrin/cysteine-rich (MDC) domains of ADAM/adamalysin/reprolysin family protein VAP1 and suggested a potential protein–protein interaction site that may function in specifying target proteins [11]. Among the family proteins, RVV-X is unique in having CLP domains within the molecule and a strict substrate specificity. To extend our understanding of the protein–protein interactions and target specificity of this family of proteins, we determined the crystal structure of RVV-X. Here, we report the crystal structure of RVV-X at 2.9 Å resolution and present a factor X docking model.

2. Materials and methods

RVV-X was purchased from Enzyme Research Laboratories Inc. and was further purified using a CM Hi-Trap column (GE healthcare Bio-Science Corp.) in the presence of GM6001 (*N*-[(2*R*)-2-(hydroxamidocarbonyllethyl)-4-methylpentanoyl]-L-tryptophan methylamide (CALBIOCHEM)). Crystals were obtained by the sitting drop vapor diffusion method. Droplets were prepared by mixing 1 μl of protein solution and 1 μl of reservoir solution (0.1 M calcium acetate, 0.1 M sodium cacodylate, 10% PEG8000, pH 6.5) supplemented with one fifth volume of 10% PEG3350 and were equilibrated against 1 ml of reservoir solution at 293 K, typically for one week. Crystals were soaked in reservoir solution supplemented with 15% MPD (2-methyl-2,4-pentandiol) prior to flash cryo-cooling under a stream of nitrogen gas at 100 K.

The diffraction data set was acquired using the SPring-8 beamline BL41XU at a wavelength of 1.0 Å at 100 K. The best crystal generated a data set with a 2.9 Å resolution (Table 1). The asymmetric unit contained one RVV-X molecule. The RVV-X structure was solved by the molecular replacement method using search models constructed from acutolysin-C (1QUA), catrocollastatin/VAP2B (2DW0), and fIX-bind-

*Corresponding author. Fax: +81 6 6872 7485.
E-mail address: stakeda@ri.ncvc.go.jp (S. Takeda).

Abbreviations: RVV-X, Russell's viper venom factor X activator; ADAM, a disintegrin and metalloproteinase; MDC, metalloproteinase/disintegrin/cysteine-rich; HVR, hyper-variable-region; PEG, polyethyleneglycol

0014-5793/$32.00
doi:10.1016/j.febslet.2007.11.062

Table 1
Data collection and refinement statistics

	Crystal 1
Data collection	
Space group	$P2_12_12_1$
Cell dimensions	
a, *b*, *c* (Å)	70.4, 91.7, 152.9
α, β, γ (°)	90, 90, 90
Resolution (Å)	50–2.9 (3.0–2.9)
R_{merge}[a]	0.069 (0.212)
$I/\sigma I$	17.0 (7.0)
Completeness (%)	96.4 (79.5)
Redundancy	6.3 (5.5)
Refinement	
Resolution (Å)	44.6–2.91 (3.0–2.91)
No. reflections	21482 (1661)
R_{work}[b]/R_{free}[c]	0.218/0.273
No. atoms	
Protein	5300
Zn^{2+}	1
Ca^{2+}	5
carbohydrate	106
GM6001	28
R.m.s deviations	
Bond lengths (Å)	0.0045
Bond angles (°)	1.12

Highest resolution shell is shown in parenthesis.
[a] $R_{merge} = \sum_{hkl}\sum_i |I_i(hkl) - \langle I(hlk)\rangle| / \sum_{hkl}\sum_i I_i(hkl)$, where $I_i(hkl)$ is the *i*th intensity measurement of reflection *hkl* and $\langle I(hlk)\rangle$ is its average.
[b] $R_{work} = \sum(\| F_{obs}| - |F_{calc}\|) / \sum|F_{obs}|$.
[c] R_{free} = *R*-value for a randomly selected subset (5%) of the data that were not used for minimization of the crystallographic residual.

ing protein (IX-bp, 1J34), for the M, C and CLP domains, respectively. The final model includes amino acid residues 7-422 of the heavy chain, 1-59 and 64-133 of light chain-A (LA) and 3-123 of light chain-B (LB), and was refined to a resolution of 2.9 Å (Table 1). The overall resolution is not particularly high when compared to those of the other snake venom protein structures, most likely due to the relatively high solvent content of the crystal (~60%) and the flexible modular architecture of the MDC domains [12]. However, well-determined structural models for most sub-domains generated the electron-density maps that enable us to build a reliable model. The overall B-factor is relatively high (average B-factor of the total protein atoms is 72.2 Å^2) and the electron-densities associated with the charged side-chains located on the molecular surface (61 aa corresponding to 9% of the total model of 672 aa) are not clearly observed, however, almost all of the side-chains inside the molecule are defined in the final electron-density maps (Fig. 1B and C). Details of preparation, crystallization and structural analysis are described in the Supplementary information.

3. Results and discussion

3.1. Overall structure of RVV-X

The overall structure of RVV-X resembles a hook-spanner-wrench configuration, where the major portion of the heavy chain forms a hook and the remaining heavy chain portion and the light chains form a handle (Fig. 1A). The backbone structure of the heavy chain is essentially the same as each monomer of VAP1 [11] and catrocollastain/VAP2B [12], with the exception of the sub-domain orientations (Fig. 1D and E). There are direct, but less-specific interactions between the M and C domains, most likely resulting from crystal packing forces, such that the entire RVV-X MDC domain forms a closed C-shape structure, unlike the open C-shaped structures of VAP1 and catrocollastain/VAP2B. The M domain of RVV-X has a flat elliptical shape with a core formed by a five-stranded β-sheet and five α-helices and contains the conserved Zn^{2+}-binding HEXXHXXGXXHD sequence (residues 145–156) and a "Met-tern" (Met169) bearing the typical structural features of the metzincin family of metalloproteinases [13]. RVV-X has a fourth disulfide bridge (Cys27-Cys63) (Fig. 1B), in addition to the three conserved disulfide bridges (Cys120-Cys200, Cys160-Cys184 and Cys162-Cys167) [4] in the M domain. The M domain is followed by the D and C domains, which are further divided into shoulder (D_s), arm (D_a), wrist (C_w) and hand (C_h), segments, and the entire heavy chain folds into a C-shaped structure (Fig. 1A). The heavy chain contains three structural Ca^{2+}-binding sites and a number of disulfide bridges (9 and 5 in the D and C domains, respectively) that are highly conserved among the ADAM/adamalysin/reprolysin family proteins [11,12].

The two homologous light chains have a fold similar to the carbohydrate-recognition domain (CRD) of rat mannose binding protein (MBP) [14], but they form an intertwined dimer where the central portion of each chain projects toward the adjoining subunit (Fig. 1A). The light chains are related by a pseudo 2-fold axis which is perpendicular to the long axis of the light chain dimer.

3.2. (HVR)-mediated protein–protein interaction

RVV-X has a unique cysteine residue (Cys389) in the middle of the hyper-variable-region (HVR, residues 373–394) in C_h, a putative protein–protein interaction site for this family of proteins [11]. Cys389 forms a disulfide bond with the C-terminal cysteine residue (Cys133) of LA (Fig. 1A and C). Aside from this inter-chain disulfide bridge, Tyr346, Tyr347, and Met385 in the heavy chain form multiple hydrophobic interactions and hydrogen bonds with Tyr11, Phe12, and Pro131 in LA, which further stabilize the continuous C_h/LA structure (Fig. 1C). Most of these residues involved in the interaction between C_h and LA are not conserved among ADAMs [11,12] or among other CLPs [10]. The RVV-X structure represents the first example of HVR-mediated protein–protein interactions by the ADAM/adamalysin/reprolysin family proteins.

3.3. Light chains

Both the overall structure and the surface features of the RVV-X light chains are quite similar to those of the factor X-binding protein (X-bp) from *Deinagkistrodon actus* venom (the r.m.s. deviation of the 240 equivalent Cα atoms is 2.6 Å) determined in complex with the γ-carboxyglutamic acid (Gla) domain of factor X [15] (Fig. 2A and B). X-bp has strong anticoagulant activities because it binds to the Gla domain of factor X and inhibits its membrane-anchoring function [16]. The hydrophobic residues that are critical for the membrane-anchoring function of factor X (Phe4, Leu5 and Val8) interact with the hydrophobic patch formed by the hydrophobic residues (Met113, Ile114 and Ala115) of the B chain in X-bp [15]. Those residues are conserved in RVV-X (Phe114, Ile115 and Ala116 of LB) (Fig. 2B). The positively charged patches on X-bp that directly interact with the Gla residues in factor X are conserved, but, are less prominent in RVV-X because of amino acid substitutions (especially, Ile101 and Glu104) (Fig. 2B). The structural similarities between the RVV-X light chains and X-bp suggest the intriguing possibility that RVV-X recognizes the factor X Gla domain through an exosite, formed by the light chains (Fig. 2C).

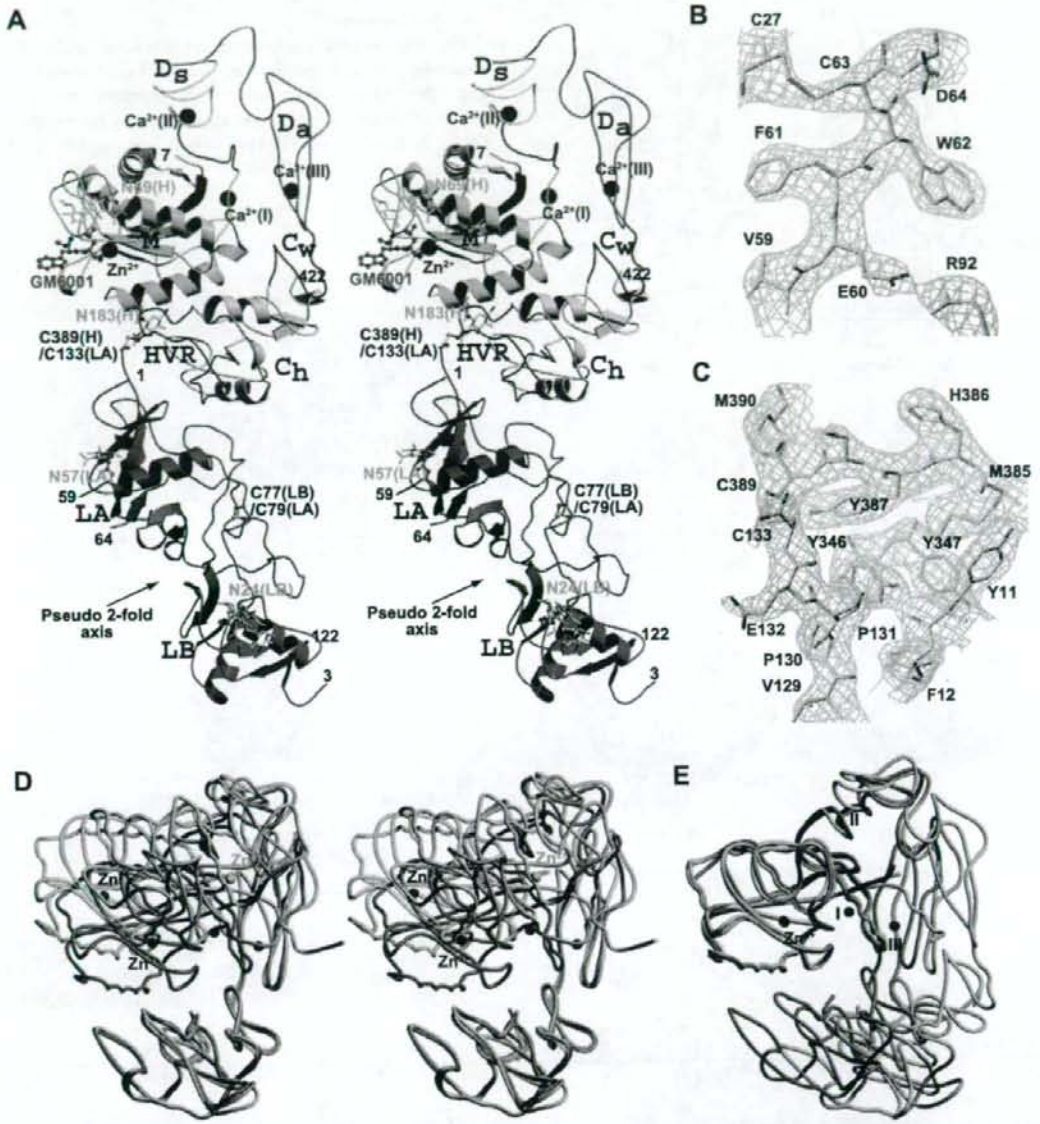

Fig. 1. Structure of RVV-X. (A) Ribbon structure of RVV-X in stereo. Bound calcium and zinc ions are represented by black and red spheres, respectively. The carbohydrate moieties (in green) linked to asparagine residues and GM6001 (in magenta) are shown in ball-and-stick representations. $2F_o - F_c$ electron-density maps (1.0σ) around the disulfide bridge between Cys27(HC) and Cys63(HC), and between Cys389 (HC) and Cys133 (LA) are represented in (B) and in (C), respectively. The HC and LA residues are labelled in black and in red, respectively. (D) Superimposition of the C_h segment of the RVV-X heavy chain (in pink) with that of the VAP1 monomer (chain-A in 2ERO, in yellow), and with that of the catrocollastatin/VAP2B (chain-A in 2DW0, in cyan) in stereo. The bound zinc and calcium atoms in RVV-X are shown as red and black spheres, respectively. The zinc atoms in VAP1 and catrocollastain/VAP2B are shown as green and blue spheres, respectively. (E) Superimposition of the M domain of the RVV-X heavy chain with the M domains of the VAP1 monomer and catrocollastatin/VAP2B.

When a properly folded Gla domain is absent from factor X, the rate of factor X activation by RVV-X is markedly diminished. In the acarboxy factor X, in which Gla formation has been blocked by a vitamin K antagonist [17] or the Des (1-44) factor X [18], factor X activation occurs at less than 1% of the rate of native factor X. Activation of factor X by RVV-X is dramatically enhanced by millimolar Ca^{2+}, which induces a conformational change in the Gla domain that enhances its binding to RVV-X [19]. Moreover, RVV-X catalyzed factor X activation is inhibited by X-bp [7]. Collectively, these observations suggest that the concave cleft created between the two light chains in RVV-X may function as an exosite for factor X-binding.

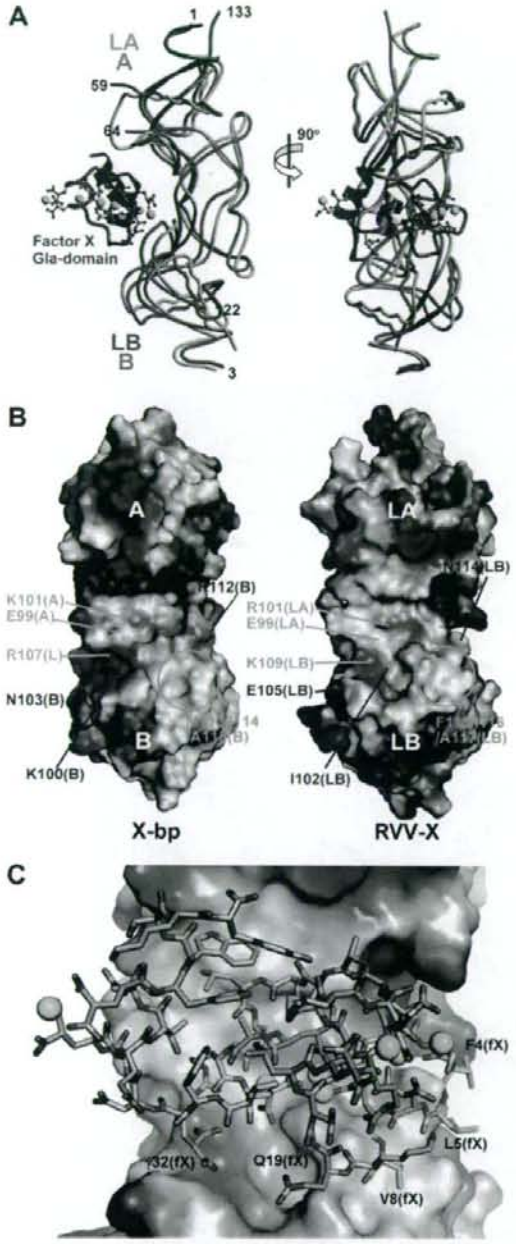

Fig. 2. Comparison of the RVV-X light chains and X-bp. (A) Superimposition of the RVV-X light chains (LA in orange and LB in magenta) onto the structure of X-bp (in gray) in complex with the Gla domain (in pink) of factor Xa (1IOD). The Gla residues and the Ca^{2+} ions are shown in ball-and-stick representation and as green spheres, respectively. (B) The molecular surfaces of X-bp and the light chains of RVV-X are represented according their electrochemical potentials (blue for positive, red for negative) and are viewed from the pseudo 2-fold axis. Conserved and varied residues are labelled in cyan and in red, respectively. (C) A model of the RVV-X light chains in complex with the Gla domain that was positioned based on the X-bp/fX Gla domain complex structure.

3.4. Docking model

Fig. 3A represents a preliminary docking model. For constructing a model, firstly, the second EGF domain (EGF2) and the serine proteinase (SP) domain of factor Xa (PDBID:1XKA) were placed such that the N-terminus of the factor X heavy chain (Ile195) closely approaches the RVV-X active site, and the globular SP domain fits into the concave

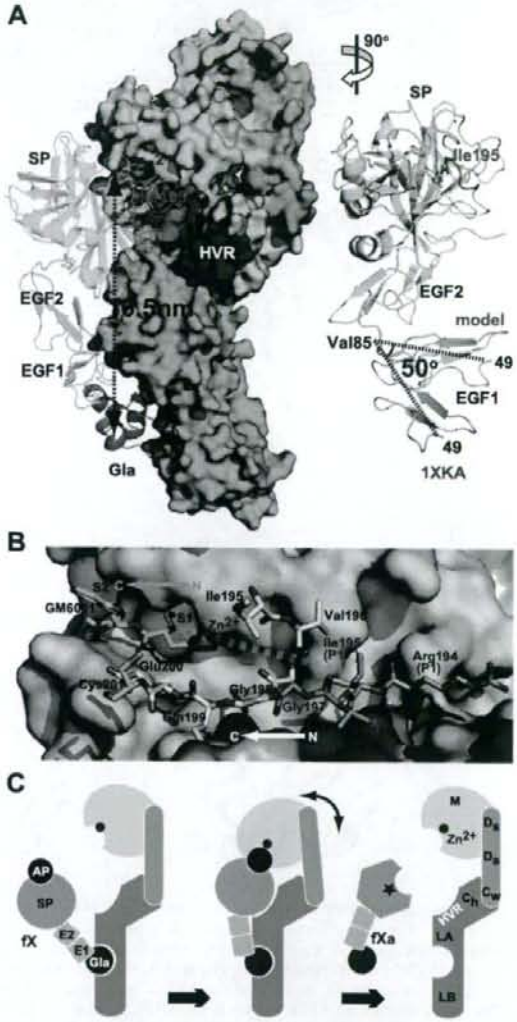

Fig. 3. Docking model. (A) The surfaces of the RVV-X sub-domains are coloured as in Fig. 1A. Factor Xa is shown in ribbon representation. Ile195 (in stick representation) and the N-terminal region (residues 195-201) of the factor X heavy chain are shown in magenta. In the right panel, the EGF1 segment of the original structural model (1XKA) is shown in gray. (B) Close up view of the RVV-X catalytic site of the docking model viewed from inside the factor Xa molecule. The N-terminal residues of factor Xa are shown in white and those of the model of factor X (zymogen) are shown in light pink. Because the factor X structure is currently unavailable, we assumed that this region has an extended structure. (C) Schematic model of factor X activation by RVV-X.

surface created by the C_h/LA domains. Secondly, we introduced a 50° bend between the two EGF domains so that the EGF1 domain fits to the convex surface of the LA domain (Fig. 3A). The linker between the two EGF domains is most likely flexible in solution [20]. This displacement successfully placed the N-terminus of the EGF1 domain in close proximity to the C-terminus of the Gla domain.

In the factor Xa structure, the N-terminal residue of the heavy chain, Ile195, is buried within the protein [20]. However, in the zymogen, the intact Arg194-Ile195-containing segment must be situated on the molecular surface, as in the equivalent segments of other serine proteinase zymogen structures [21]. The region of factor X that is C-terminal to the scissile peptide (segment coloured in magenta in Fig. 3A) may be located along the surface of the SP domain, resulting in its binding to the primed region of RVV-X, in the same orientation as the peptide-like inhibitor GM6001 lies in the current crystal structure (Fig. 3B). In the present docking model, since both molecules were positioned just as a rigid body without any collision, the active site zinc atom of RVV-X and Ile195 of factor Xa are 16 Å apart. Intrinsic hinge motions of the modular M/D_s/D_a/C_w architecture [12], and conformational changes upon association of RVV-X and the factor X zymogen, may allow the catalytic site of RVV-X to interact directly with the Arg194-Ile195 bond of factor X when in solution (Fig. 3C). The relatively large separation (~65 Å) of the catalytic site and the Gla-domain-binding exosite may explain the high specificity of RVV-X for factor X.

3.5. Implication for molecular evolution of RVV-X

CLPs from snake venoms are characterized by a unique dimerization mechanism of protein evolution, in which two monomers swap a portion of the long loop region, forming a stable functional unit and creating a new concave surface for target binding for a variety of biological activities [10]. Dimers can further aggregate with each other to form higher-order oligomers [22], or, as in the case of RVV-X, form covalently linked complexes with a metalloproteinase chain creating an exosite. The RVV-X structure illustrates a good example of evolutionary gain of function by multi-subunit proteins, represented by the fold adaptation, for the binding of other ligands.

4. Conclusion

ADAMs are widely distributed and constitute the major membrane-bound sheddases to play roles in important processes occurring at the cell surface. However, the molecular mechanism of target recognition by ADAMs and which ADAMs shed which key substrates in specific biological events has been poorly understood. Previously, we suggested that the HVR may constitute an exosite that captures the target or associated proteins, and that is processed by the catalytic site [11]. The RVV-X structure is consistent with this model and provides insights into the molecular basis of HVR-mediated protein–protein interactions and target recognition by ADAM/adamalysin/reprolysin family proteins.

Acknowledgements: The authors thank M. Tomisako for help in crystallization experiments, M. Kawamoto and N. Shimizu for assistance with data acquisition at the SPring-8 beamline BL41XU and T. Morita for helpful discussions. This work was partly supported by the Ministry of Education, Science, Sports and Culture, Grant-in-aid for Scientific Research B-19370047-2007, and Health and Labor Science Research Grants, and by grants from the Mitsubishi Pharma Research Foundation and the Astellas Foundation for Research on Metabolic Disorders. T.I is supported by the grant from New Energy and Industrial Technology Development Organization (NEDO) of Japan.

Appendix A. Supplementary data

The atomic coordinates and structure factors have been deposited in the NCBI protein data bank with the accession code 2E3X. Supplementary data associated with this article can be found, in the online version, at doi:10.1016/j.febslet.2007.11.062.

References

[1] Mann, K.G., Nesheim, M.E., Church, W.R., Haley, P. and Krishnaswamy, S. (1990) Surface-dependent reactions of the vitamin K-dependent enzyme complexes. Blood 76, 1–16.
[2] Morita, T. (1998) Proteases which activate factor X in: Enzymes from Snake Venom (Bailey, G.S., Ed.), pp. 179–208, Alaken, Colorado.
[3] Tans, G. and Rosing, J. (2001) Snake venom activators of factor X: an overview. Haemostasis 31, 225–233.
[4] Fox, J.W. and Serrano, S.M. (2005) Structural considerations of the snake venom metalloproteinases, key members of the M12 reprolysin family of metalloproteinases. Toxicon 45, 969–985.
[5] Gowda, D.C., Jackson, C.M., Hensley, P. and Davidson, E.A. (1994) Factor X-activating glycoprotein of Russell's viper venom. Polypeptide composition and characterization of the carbohydrate moieties. J. Biol. Chem. 269, 10644–10650.
[6] Kisiel, W., Hermodson, M.A. and Davie, E.W. (1976) Factor X activating enzyme from Russell's viper venom: isolation and characterization. Biochemistry 15, 4901–4906.
[7] Takeya, H., Nishida, S., Miyata, T., Kawada, S., Saisaka, Y., Morita, T. and Iwanaga, S. (1992) Coagulation factor X activating enzyme from Russell's viper venom (RVV-X). A novel metalloproteinase with disintegrin (platelet aggregation inhibitor)-like and C-type lectin-like domains. J. Biol. Chem. 267, 14109–14117.
[8] White, J.M. (2003) ADAMs: modulators of cell–cell and cell–matrix interactions. Curr. Opin. Cell Biol. 15, 598–606.
[9] Seals, D.F. and Courtneidge, S.A. (2003) The ADAMs family of metalloproteases: multidomain proteins with multiple functions. Genes Dev. 17, 7–30.
[10] Morita, T. (2005) Structures and functions of snake venom CLPs (C-type lectin-like proteins) with anticoagulant-, procoagulant-, and platelet-modulating activities. Toxicon 45, 1099–1114.
[11] Takeda, S., Igarashi, T., Mori, H. and Araki, S. (2006) Crystal structures of VAP1 reveal ADAMs' MDC domain architecture and its unique C-shaped scaffold. EMBO J. 25, 2388–2396.
[12] Igarashi, T., Araki, S., Mori, H. and Takeda, S. (2007) Crystal structures of catrocollastatin/VAP2B reveal a dynamic, modular architecture of ADAM/adamalysin/reprolysin family proteins. FEBS Lett. 581, 2416–2422.
[13] Gomis-Ruth, F.X. (2003) Structural aspects of the metzincin clan of metalloendopeptidases. Mol. Biotechnol. 24, 157–202.
[14] Weis, W.I., Kahn, R., Fourme, R., Drickamer, K. and Hendrickson, W.A. (1991) Structure of the calcium-dependent lectin domain from a rat mannose-binding protein determined by MAD phasing. Science 254, 1608–1615.
[15] Mizuno, H., Fujimoto, Z., Atoda, H. and Morita, T. (2001) Crystal structure of an anticoagulant protein in complex with the Gla domain of factor X. Proc. Natl. Acad. Sci. USA 98, 7230–7234.
[16] Atoda, H., Ishikawa, M., Mizuno, H. and Morita, T. (1998) Coagulation factor X-binding protein from Deinagkistrodon acutus venom is a Gla domain-binding protein. Biochemistry 37, 17361–17370.

[17] Lindhout, M.J., Kop-Klaassen, B.H. and Hemker, H.C. (1978) Activation of decarboxyfactor X by a protein from Russell's viper venom. Purification and partial characterization of activated decarboxyfactor X. Biochim. Biophys. Acta 533, 327–341.
[18] Morita, T. and Jackson, C.M. (1986) Preparation and properties of derivatives of bovine factor X and factor Xa from which the gamma-carboxyglutamic acid containing domain has been removed. J. Biol. Chem. 261, 4015–4023.
[19] Skogen, W.F., Bushong, D.S., Johnson, A.E. and Cox, A.C. (1983) The role of the Gla domain in the activation of bovine coagulation factor X by the snake venom protein XCP. Biochem. Biophys. Res. Commun. 111, 14–20.
[20] Kamata, K., Kawamoto, H., Honma, T., Iwama, T. and Kim, S.H. (1998) Structural basis for chemical inhibition of human blood coagulation factor Xa. Proc. Natl. Acad. Sci. USA 95, 6630–6635.
[21] Freer, S.T., Kraut, J., Robertus, J.D., Wright, H.T. and Xuong, N.H. (1970) Chymotrypsinogen: 2.5-angstrom crystal structure, comparison with alpha-chymotrypsin, and implications for zymogen activation. Biochemistry 9, 1997–2009.
[22] Fukuda, K., Mizuno, H., Atoda, H. and Morita, T. (2000) Crystal structure of flavocetin-A, a platelet glycoprotein Ib-binding protein, reveals a novel cyclic tetramer of C-type lectin-like heterodimers. Biochemistry 39, 1915–1923.

Journal of the American College of Cardiology
© 2007 by the American College of Cardiology Foundation
Published by Elsevier Inc.

Vol. 50, No. 13, 2007
ISSN 0735-1097/07/$32.00
doi:10.1016/j.jacc.2007.05.039

PRECLINICAL STUDIES

Important Role of Endogenous Hydrogen Peroxide in Pacing-Induced Metabolic Coronary Vasodilation in Dogs In Vivo

Toyotaka Yada, MD, PHD,* Hiroaki Shimokawa, MD, PHD,† Osamu Hiramatsu, PHD,* Yoshiro Shinozaki, BS,‡ Hidezo Mori, MD, PHD,§ Masami Goto, MD, PHD,* Yasuo Ogasawara, PHD,* Fumihiko Kajiya, MD, PHD*

Kurashiki, Sendai, Isehara, and Suita, Japan

Objectives We examined whether endogenous hydrogen peroxide (H_2O_2) is involved in pacing-induced metabolic vasodilation in vivo.

Background We have previously demonstrated that endothelium-derived H_2O_2 is an endothelium-derived hyperpolarizing factor in canine coronary microcirculation in vivo. However, the role of endogenous H_2O_2 in metabolic coronary vasodilation in vivo remains to be examined.

Methods Canine subepicardial small coronary arteries (≥100 μm) and arterioles (<100 μm) were continuously observed by a microscope under cyclooxygenase blockade (ibuprofen, 12.5 mg/kg intravenous [IV]) (n = 60). Experiments were performed during paired right ventricular pacing under the following 7 conditions: control, nitric oxide (NO) synthase inhibitor (N^G-monomethyl-L-arginine [L-NMMA], 2 μmol/min for 20 min intracoronary [IC]), catalase (a decomposer of H_2O_2, 40,000 U/kg IV and 240,000 U/kg/min for 10 min IC), 8-sulfophenyltheophylline (SPT) (an adenosine receptor blocker, 25 μg/kg/min for 5 min IC), L-NMMA+catalase, L-NMMA+tetraethylammonium (TEA) (K_{Ca}-channel blocker, 10 μg/kg/min for 10 min IC), and L-NMMA+catalase+8-SPT.

Results Cardiac tachypacing (60 to 120 beats/min) caused coronary vasodilation in both-sized arteries under control conditions in response to the increase in myocardial oxygen consumption. The metabolic coronary vasodilation was decreased after L-NMMA in subepicardial small arteries with an increased fluorescent H_2O_2 production compared with catalase group, whereas catalase decreased the vasodilation of arterioles with an increased fluorescent NO production compared with the L-NMMA group, and 8-SPT also decreased the vasodilation of arterioles. Furthermore, the metabolic coronary vasodilation was markedly attenuated after L-NMMA+catalase, L-NMMA+TEA, and L-NMMA+catalase+8-SPT in both-sized arteries.

Conclusions These results indicate that endogenous H_2O_2 plays an important role in pacing-induced metabolic coronary vasodilation in vivo. (J Am Coll Cardiol 2007;50:1272–8) © 2007 by the American College of Cardiology Foundation

Cardiac tachycardia by pacing or exercise increases myocardial oxygen consumption (MVO_2) and increases coronary blood flow by several mechanisms (1–3). Shear stress plays a crucial role in modulating vascular tone by endothelium-derived releasing factors (EDRFs), including nitric oxide (NO), prostacyclin (PGI_2), and endothelium-derived hyperpolarizing factor (EDHF) (4,5). Flow-induced vasodilation is mediated by either NO (6,7), PGI_2 (8), both of them (9), or EDHF (10). Matoba et al. have previously identified that endothelium-derived hydrogen peroxide (H_2O_2) is a primary EDHF in mesenteric arteries of mice and humans (11,12). Morikawa et al. (13,14) subsequently confirmed

See page 1279

From the *Department of Medical Engineering and Systems Cardiology, Kawasaki Medical School, Kurashiki, Japan; †Department of Cardiovascular Medicine, Tohoku University Graduate School of Medicine, Sendai, Japan; ‡Department of Physiology, Tokai University School of Medicine, Isehara, Japan; and the §Department of Cardiac Physiology, National Cardiovascular Center Research Institute, Suita, Japan. Dr. Yada is the winner of the Endothelium-Derived Hyperpolarizing Factor (EDHF) Tanabe Award from the Scientific Sessions of the American Heart Association, November 2005, Dallas, Texas. This work was supported in part by grants from the Japanese Ministry of Education, Science, Sports, Culture, and Technology, Tokyo, Japan, Nos. 16209027 (to Dr. Shimokawa) and 16300164 (to Dr. Yada), the Program for Promotion of Fundamental Studies in Health Sciences of the Organization for Pharmaceutical Safety and Research of Japan (to Dr. Shimokawa), and Takeda Science Foundation 2002 (to Dr. Yada).

Manuscript received September 11, 2006; revised manuscript received April 25, 2007, accepted May 1, 2007.

that endothelial Cu,Zn-superoxide dismutase (SOD) plays an important role as an EDHF synthase in mice and humans. Miura et al. (15) demonstrated that endothelium-derived H_2O_2 is involved as an EDHF in the flow-induced vasodilation of isolated human coronary arterioles in vitro. We have recently confirmed that endogenous H_2O_2 plays an important compensatory role during coronary autoregulation (16) and reperfusion injury in vivo (17) through the interactions with NO and adenosine.

It is known that vascular α-adrenergic receptor is modulated by the endothelium in dogs (18), whereas cardiac β-adrenergic receptor is modulated by K_{Ca} channels in pigs (19) and H_2O_2 in mice (20). However, the role of endogenous H_2O_2 in metabolic coronary vasodilation in vivo remains largely unknown. In the present study, we thus examined whether H_2O_2 is involved in pacing-induced metabolic coronary vasodilation in canine coronary microcirculation in vivo.

Methods

This study conformed to the Guideline on Animal Experiments of Kawasaki Medical School and the Guide for the Care and Use of Laboratory Animals published by the U.S. National Institutes of Health.

Animal preparation. Anesthetized mongrel dogs of either gender (15 to 25 kg in body weight, n = 60) were ventilated with a ventilator (Model VS600, IDC, Pittsburgh, Pennsylvania). We continuously monitored aortic pressure and left ventricular pressure (LVP) with a catheter (SPC-784A, Millar, Houston, Texas) and blood flow of the left anterior descending coronary artery (LAD) with a transonic flow probe (T206, Transonic Systems, Ithaca, New York).

Measurements of coronary diameter by intravital microscope. We continuously monitored coronary vascular responses by an intravital microscope (VMS 1210, Nihon Kohden, Tokyo, Japan) with a needle-probe in vivo, as previously described (21). We gently placed the needle-probe on subepicardial microvessels. When a clear vascular image was obtained, end-diastolic vascular images were taken with 30 pictures/s (21).

Measurements of regional myocardial blood flow. Regional myocardial blood flow was measured by the nonradioactive microsphere (Sekisui Plastic Co. Ltd., Tokyo, Japan) technique, as previously described (22). Briefly, the microspheres suspension was injected into the left atrium 3 min after tachypacing. Myocardial flow in the LAD area was calculated according to the formula "time flow = tissue counts × (reference flow/reference counts)" and was expressed in ml/g/min (22).

Detection of H_2O_2 and NO production in coronary microvessels. 2′,7′-dichlorodihydrofluorescein diacetate (DCF) (Molecular Probes, Eugene, Oregon) and diaminorhodamine-4M AM (DAR) (Daiichi Pure Chemicals, Tokyo, Japan) were used to detect H_2O_2 and NO production in coronary microvessels, respectively, as previously described (17). Briefly, fresh and unfixed heart tissues were cut into several blocks and immediately frozen in optimal cutting temperature compound (Tissue-Tek, Sakura Fine Chemical, Tokyo, Japan). Fluorescent images of the microvessels were obtained 3 min after application of acetylcholine (ACh) by using a fluorescence microscope (OLYMPUS BX51, Tokyo, Japan) (17).

Experimental protocols. After the surgical procedure and instrumentation, at least 30 min were allowed for stabilization while monitoring hemodynamic variables. Coronary vasodilator responses were examined before and after cardiac tachypacing (60 to 120 beats/min) under the following 7 conditions with cyclooxygenase blockade (ibuprofen, 12.5 mg/kg, IV) to evaluate the role of H_2O_2 and NO without PGI_2 in a different set of animals (Fig. 1): 1) control conditions without any inhibitor; 2) L-NMMA alone (2 μmol/min intracoronary [IC] for 20 min); 3) catalase alone (40,000 U/kg intravenous [IV] and 240,000 U/kg/min IC for 10 min, an enzyme that dismutates

Abbreviations and Acronyms

CBF = coronary blood flow
DAR = diaminorhodamine-4M AM
DCF = 2′,7′-dichlorodihydrofluorescein diacetate
EDHF = endothelium-derived hyperpolarizing factor
H_2O_2 = hydrogen peroxide
L-NMMA = N^G-monomethyl-L-arginine
LAD = left anterior descending coronary artery
MVO_2 = myocardial oxygen consumption
NO = nitric oxide
PGI_2 = prostacyclin
SPT = sulfophenyltheophylline
TEA = tetraethylammonium

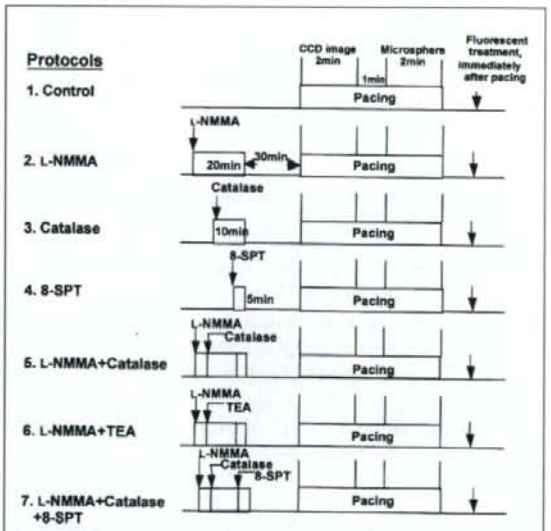

Figure 1 Experimental Protocols

CCD = charge-coupled device; L-NMMA = N^G-monomethyl-L-arginine; SPT = sulfophenyltheophylline; TEA = tetraethylammonium.

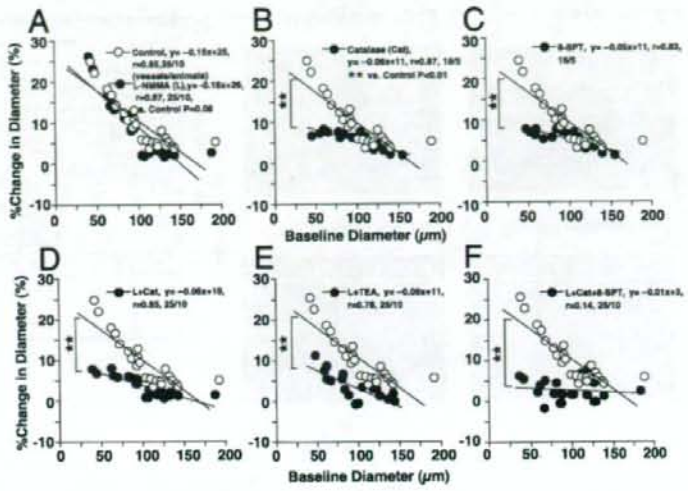

Figure 2 Coronary Vascular Responses to Cardiac Pacing

The coronary vasodilating responses of both-sized coronary arteries were significantly inhibited in all experimental conditions except L-NMMA alone. **p < 0.01. Abbreviations as in Figure 1.

H_2O_2 into water and oxygen); 4) adenosine receptor blockade alone (8-sulfophenyltheophylline [8-SPT], 25 μg/kg/min IC for 5 min); 5) catalase plus L-NMMA; 6) catalase plus tetraethylammonium (TEA) (10 μg/kg/min IC for 10 min, an inhibitor of large conductance K_{Ca} channels to inhibit EDHF-mediated responses) (23); and 7) catalase plus L-NMMA with 8-SPT (16). These inhibitors were given at 30 min before cardiac tachypacing (Fig. 1). The basal coronary diameter was defined as that before pacing. We continuously observed the diameter change in subepicardial small coronary arteries (≥100 μm) and arterioles (<100 μm) with an intravital microscope before and at 2 min after pacing. Microspheres were administered at 3 min after the pacing was started (Fig. 1). In the combined infusion protocol (L-NMMA+catalase+8-SPT), L-NMMA infusion was first started, followed by catalase infusion, and then 8-SPT was added at 15 min after the initiation of L-NMMA infusion (Fig. 1). Then, fresh and unfixed heart tissues were cut into several blocks and immediately frozen in optimal cutting temperature compound after the pacing. The flow and MVO_2 were measured as full-thickness values.

Drugs. All drugs were obtained from Sigma Chemical Co. and were diluted in a physiological saline immediately before use.

Statistical analysis. Results are expressed as means ± SEM. Differences in the vasodilation of subepicardial coronary microvessels before and after pacing (Fig. 2) were examined by a multiple regression analysis using a model, in which the change in coronary diameter was set as a dependent variable (y) and vascular size as an explanatory variable (x), while the statuses of control and other inhibitors were set as dummy variables (D1, D2) in the following equation: y = a0 + a1x + a2D1 + a3D2, where a0 through a3 are partial regression coefficients (16). Significance tests were made as simultaneous tests for slope and intercept differences. Pairwise comparisons against control were made without adjustment for multiple comparisons. The vessel was the unit of analysis without correction for correlated observations. The power of this analysis is greater than that of using the animal as the unit of analysis, giving smaller p values. Vascular fluorescent responses (Figs. 3 and 4) were analyzed by one-way analysis of variance followed by Scheffe's post hoc test for multiple comparisons. The criterion for statistical significance was at $p < 0.05$.

Results

Hemodynamic status and blood gases during pacing. Throughout the experiments, mean aortic pressure was constant and comparable (Table 1), and pO_2, pCO_2, and pH were maintained within the physiological ranges (pO_2 >70 mm Hg, pCO_2 25 to 40 mm Hg, and pH 7.35 to 7.45). Baseline coronary diameter was comparable in the absence and presence of inhibitors under the 7 different experimental conditions (Table 1). Cardiac tachypacing increased coronary blood flow and MVO_2 from the baseline values (Table 2, both $p < 0.01$). Combined infusion of L-NMMA+catalase+8-SPT significantly decreased coronary blood flow (CBF) and MVO_2 as compared with control, L-NMMA alone (both $p < 0.01$), catalase alone (both $p < 0.01$), 8-SPT alone (both $p < 0.01$), L-NMMA+catalase (both $p < 0.05$), L-NMMA+TEA (both $p < 0.05$). Com-

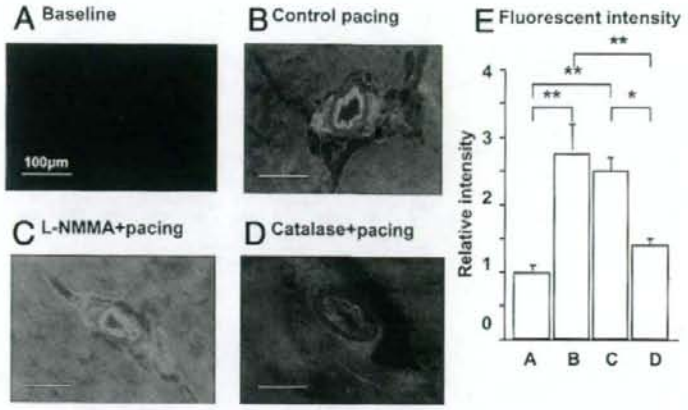

Figure 3 Detection of H_2O_2 Production With DCF Fluorescent Method

Hydrogen peroxide (H_2O_2) production was unaltered after N^G-monomethyl-L-arginine (L-NMMA) but was markedly suppressed by catalase. Number of arterioles/animals used was 5/5 for each group. *p < 0.05, **p < 0.01. DCF = 2',7'-dichlorodihydrofluorescein diacetate.

bined infusion of L-NMMA+catalase or L-NMMA+TEA significantly decreased CBF (both $p < 0.05$) and MVO_2 (both $p < 0.05$) as compared with control after the pacing.

Coronary vasodilation before and after cardiac tachypacing. Cardiac tachypacing caused coronary vasodilation in both-sized arteries under control conditions (small coronary arteries, 5 ± 1%; arterioles, 14 ± 2%) (Fig. 2A) with decreased coronary venous pO_2 (Table 2). The metabolic coronary vasodilation was significantly decreased after L-NMMA in small coronary arteries (3 ± 1%) but not in arterioles (14 ± 2%), whereas catalase and 8-SPT decreased the vasodilation of arterioles (both 4 ± 1%) but not in small coronary arteries (both 7 ± 1%) (Figs. 2B and 2C). Furthermore, the metabolic coronary vasodilation was markedly attenuated after L-NMMA+catalase and L-NMMA+TEA in small coronary arteries (both 2 ± 1%), and L-NMMA+catalase+8-SPT almost abolished the vasodilating responses in both-sized arteries (small coronary arteries, −1 ± 1%; arterioles, 1 ± 1%) (Figs. 2D to 2F). When expressed in a linear regression analysis, the coronary vasodilating responses of both-sized coronary arteries were significantly inhibited in all experimental conditions except L-NMMA alone (Fig. 2A).

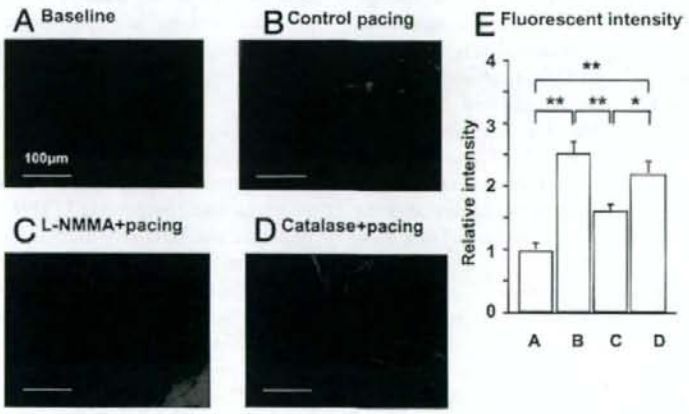

Figure 4 Detection of NO Production With DAR Fluorescent Method

Nitric oxide (NO) production was unaltered after catalase but was markedly suppressed by N^G-monomethyl-L-arginine (L-NMMA). Number of arterioles/animals used was 5/5 for each group. *p < 0.05, **p < 0.01. DAR = diaminorhodamine-4M AM.

JACC Vol. 50, No. 13, 2007
September 25, 2007:1272–8

Table 1 The Small Artery and Arteriolar Diameter Measurements at Rest and During Cardiac Pacing

	Control	L-NMMA (L)	Catalase (Cat)	8-SPT	L+Cat	L+TEA	L+Cat+8-SPT
Small artery							
n (vessels/dogs)	12/10	12/10	9/5	7/5	12/10	12/10	12/10
Rest (μm)	127 ± 7	125 ± 6	127 ± 5	126 ± 6	125 ± 7	123 ± 6	124 ± 7
Cardiac pacing (μm)	134 ± 7*	129 ± 7†	132 ± 5*	131 ± 6*	127 ± 7	124 ± 6	123 ± 6
Arteriole							
n (vessels/dogs)	12/10	12/10	9/5	9/5	12/10	12/10	12/10
Rest (μm)	75 ± 5	73 ± 5	71 ± 5	71 ± 5	72 ± 5	74 ± 5	72 ± 6
Cardiac pacing (μm)	85 ± 5*	82 ± 5*	77 ± 6†	77 ± 6†	77 ± 5†	77 ± 5	73 ± 5

Results are expressed as mean ± SEM. *$p < 0.01$, †$p < 0.05$ versus rest.
L-NMMA = N^G-monomethyl-L-arginine; SPT = sulfophenyltheophylline; TEA = tetraethylammonium.

Detection of H_2O_2 and NO production. Fluorescent microscopy with DCF showed that cardiac tachypacing increased coronary H_2O_2 production compared with baseline conditions in arterioles (Fig. 3). The pacing-induced H_2O_2 production as assessed by DCF fluorescent intensity was unaltered after L-NMMA but was markedly suppressed by catalase (Fig. 3). By contrast, in small coronary arteries, vascular NO production as assessed by DAR fluorescent intensity was significantly increased in response to the pacing compared with baseline conditions (Fig. 4). The pacing-induced NO production was unaltered after catalase but was markedly suppressed by L-NMMA (Fig. 4). Pacing caused no significant increase in H_2O_2 production in small coronary arteries or NO production in arterioles (data not shown).

Discussion

The major finding of the present study is that endogenous H_2O_2 plays an important role in pacing-induced metabolic coronary dilation as a compensatory mechanism for NO in vivo. We demonstrated the important role of endogenous H_2O_2 in the mechanisms for metabolic coronary dilation in vivo.

Validations of experimental model and methodology. We chose, on the basis of our previous reports (16,17), the adequate dose of L-NMMA, catalase, TEA, and 8-SPT in order to inhibit NO synthesis, H_2O_2, K_{Ca} channels, and the adenosine receptor, respectively. The TEA at low doses is fairly specific for K_{Ca} channel, but at higher doses it might block a number of other K channels. Because several K_{Ca} channels might be involved in H_2O_2-mediated responses (5), we selected nonselective K_{Ca} inhibitor, TEA, to inhibit all K_{Ca} channels (23). We have previously confirmed the validity of our present methods (21).

Role of NO and H_2O_2 after cardiac pacing. Matoba et al. have demonstrated that endothelium-derived H_2O_2 is an EDHF in mouse (11) and human (12) mesenteric arteries and pig coronary microvessels (24). Morikawa et al. also

Table 2 Hemodynamic Status at Rest and During Cardiac Pacing

	Control	L-NMMA (L)	Catalase (Cat)	8-SPT	L+Cat	L+TEA	L+Cat+8-SPT
n (dogs)	10	10	5	5	10	10	10
SBP							
Rest (mm Hg)	135 ± 14	135 ± 14	114 ± 9	123 ± 5	98 ± 9	99 ± 9	96 ± 8
Cardiac pacing	137 ± 14	136 ± 14	125 ± 12	130 ± 7	100 ± 9	100 ± 8	103 ± 9
MBP							
Rest (mm Hg)	117 ± 10	117 ± 10	98 ± 8	99 ± 5	89 ± 10	90 ± 10	87 ± 9
Cardiac pacing	124 ± 9	120 ± 13	107 ± 10	110 ± 7	91 ± 10	92 ± 10	92 ± 10
DP							
Rest	8,100 ± 845	8,100 ± 845	6,855 ± 527	7,350 ± 312	5,880 ± 537	5,910 ± 527	5,730 ± 478
Cardiac pacing	16,440 ± 1,718*	16,320 ± 1,680*	15,000 ± 1,423*	15,630 ± 778*	11,940 ± 11,029*	12,000 ± 1,011*	12,300 ± 1,078*
$CVPO_2$							
Rest (mm Hg)	20 ± 1	17 ± 1	16 ± 1	17 ± 1	15 ± 1†	15 ± 1†	14 ± 1†
Cardiac pacing	14 ± 1*	11 ± 1*	11 ± 1*	12 ± 1*	10 ± 1*†	10 ± 1*†	9 ± 1*†
MVO_2							
Rest (μlO_2/min/g)	70 ± 2	66 ± 2	67 ± 2	73 ± 5	62 ± 5	61 ± 5	60 ± 5
Cardiac pacing	171 ± 4‡	168 ± 2‡	158 ± 12‡	168 ± 13‡	133 ± 4†‡	130 ± 18†‡	95 ± 9*§
CBF							
Rest (ml/min/g)	0.66 ± 0.06	0.63 ± 0.06	0.66 ± 0.03	0.66 ± 0.01	0.59 ± 0.06	0.62 ± 0.05	0.51 ± 0.04
Cardiac pacing	1.48 ± 0.32‡	1.46 ± 0.06‡	1.36 ± 0.02‡	1.40 ± 0.01‡	1.22 ± 0.01†‡	1.24 ± 0.12†‡	0.96 ± 0.07‡§

Results are expressed as mean ± SEM. *$p < 0.05$ versus at rest. †$p < 0.05$ versus corresponding control measurements. ‡$p < 0.01$ versus rest. §$p < 0.01$ versus corresponding control measurements.
CBF = coronary blood flow; $CVPO_2$ = coronary venous pO_2; DP = double product; MBP = mean blood pressure; MVO_2 = myocardial oxygen consumption; SBP = systolic blood pressure; other abbreviations as in Table 2.

have demonstrated that endothelial Cu,Zn-SOD plays an important role as an H_2O_2/EDHF synthase in mouse (13) and human (14) mesenteric arteries. Subsequently, we (16,17) and others (15) confirmed that endogenous H_2O_2 exerts important vasodilator effects in canine coronary microcirculation in vivo and in isolated human coronary microvessels, respectively. In the present study, the pacing-induced metabolic coronary vasodilation was significantly decreased after L-NMMA in small coronary arteries but not in arterioles, whereas catalase decreased the vasodilation of arterioles but not that of small arteries, and the coronary vasodilation was markedly attenuated after L-NMMA+catalase (Fig. 2). These findings indicate that NO and H_2O_2 compensate for each other to maintain coronary vasodilation in response to increased myocardial oxygen demand. Coronary venous pO_2 tended to be lower after L-NMMA+catalase, suggesting that NO and H_2O_2 coordinately cause coronary vasodilation during cardiac tachypacing.

Saitoh et al. (25) suggested that the production of H_2O_2, which stems from the dismutation of $\cdot O_2^-$ that is formed during mitochondrial electron transport, is seminal in the coupling between oxygen metabolism and blood flow in the heart. Thus, the contribution of H_2O_2 production in response to the change in metabolism cannot be excluded.

Endothelial Cu,Zn-SOD plays an important role in the synthesis of H_2O_2 as an EDHF synthase in mouse (13) and human (14) mesenteric arteries, and exercise training enhances expression of Cu,Zn-SOD in normal pigs (26). It remains to be examined whether exercise-induced upregulation of Cu,Zn-SOD enhances metabolic coronary vasodilation mediated by endogenous H_2O_2.

Compensatory vasodilator mechanism among H_2O_2, NO, and adenosine. The EDHF acts as a partial compensatory mechanism to maintain endothelium-dependent vasodilation in the forearm microcirculation of patients with essential hypertension, where NO activity is impaired owing to oxidative stress (27). We have recently demonstrated in the fluorescent microscopy study that coronary vascular production of H_2O_2 and NO is enhanced after myocardial ischemia/reperfusion in small coronary arteries and arterioles, respectively (17). In the present study, the DCF fluorescent intensity was comparable between control and L-NMMA, and that of DAR was also comparable between control and catalase (Figs. 3 and 4). Although the exact source of vascular production of H_2O_2 and NO remains to be elucidated, it is highly possible that endothelium-derived NO and H_2O_2 compensate for each other to maintain coronary vasodilation in response to increased MVO_2.

In the dog, blockade of any vasodilator mechanisms fails to blunt the increase in coronary blood flow in response to exercise, indicating that adenosine, K^+_{ATP}-channel opening, prostanoids, or NO might not be mandatory for exercise-induced coronary vasodilation, or that these redundant vasodilator mechanisms compensate for each other when one mechanism is blocked (28). In the present study, adenosine blockade with 8-SPT alone inhibited the pacing-induced vasodilation of arteriole but not that of small artery, whereas combined administration of L-NMMA+catalase+8-SPT almost abolished the pacing-induced coronary vasodilation of both-sized arteries with an increase in coronary blood flow (Fig. 2). The discrepancy between the diameter and flow responses is likely due to the metabolic autoregulation of smaller arterioles. These results indicate that adenosine also plays an important role to maintain metabolic coronary vasodilation in cooperation with NO and H_2O_2, a finding consistent with our previous study on coronary autoregulatory mechanisms (15).

Study limitations. Several limitations should be mentioned for the present study. First, although we were able to demonstrate the production of H_2O_2 with fluorescent microscopy with DCF, we were unable to quantify the endothelial H_2O_2 production, because DCF reacts with H_2O_2, peroxynitrite, and hypochlorous acid (13). Second, we were unable to find smaller arterioles, owing to the limited spatial resolution of our charge-coupled device intravital microscope. With an intravital camera with higher resolution, we would be able to observe coronary vasodilation of smaller arterioles. Third, we were unable to determine whether H_2O_2 is produced by shear stress or cardiac metabolism. This point remains to be elucidated in a future study.

Conclusions

We were able to demonstrate that endogenous H_2O_2 plays an important role in pacing-induced metabolic coronary vasodilation in canine coronary microcirculation in vivo and that there are substantial compensatory interactions among NO, H_2O_2, and adenosine to maintain metabolic coronary vasodilation, which is one of the most important mechanisms for cardiovascular homeostasis in vivo.

Reprint requests and correspondence: Dr. Toyotaka Yada, Department of Medical Engineering and Systems Cardiology, Kawasaki Medical School, 577 Matsushima, Kurashiki, Okayama 701-0192, Japan. E-mail: yada@me.kawasaki-m.ac.jp.

REFERENCES

1. Ishibashi Y, Duncker DJ, Zhang J, Bache RJ. ATP-sensitive K^+ channels, adenosine, and nitric oxide-mediated mechanisms account for coronary vasodilation during exercise. Circ Res 1998;82:346–59.
2. Jones CJ, Kuo L, Davis MJ, DeFily DV, Chilian WM. Role of nitric oxide in the coronary microvascular responses to adenosine and increased metabolic demand. Circulation 1995;91:1807–13.
3. Yada T, Richmond KN, Van Bibber R, Kroll K, Feigl EO. Role of adenosine in local metabolic coronary vasodilation. Am J Physiol 1999;276:H1425–33.
4. Feletou M, Vanhoutte PM. Endothelium-dependent hyperpolarization of canine smooth muscle. Br J Pharmacol 1988;93:515–24.
5. Shimokawa H. Primary endothelial dysfunction: atherosclerosis. J Mol Cell Cardiol 1999;31:23–37.
6. Kuo L, Davis MJ, Chilian WM. Endothelium-dependent, flow-induced dilation of isolated coronary arterioles. Am J Physiol 1991; 259:H1063–70.

7. Kuo L, Chilian WM, Davis MJ. Interaction of pressure- and flow-induced responses in porcine coronary resistance vessels. Am J Physiol 1991;261:H1706–15.
8. Koller A, Sun D, Kaley G. Role of shear stress and endothelial prostaglandins in flow- and viscosity-induced dilation of arterioles in vitro. Circ Res 1993;72:1276–84.
9. Koller A, Sun D, Huang A, Kaley G. Corelease of nitric oxide and prostaglandins mediates flow-dependent dilation of ratgracilis muscle arterioles. Am J Physiol 1994;267:H326–32.
10. Takamura Y, Shimokawa H, Zhao H, et al. Important role of endothelium-derived hyperpolarizing factor in shear stress-induced endothelium-dependent relaxations in the rat mesenteric artery. J Cardiovasc Pharmacol 1999;34:381–7.
11. Matoba T, Shimokawa H, Nakashima M, et al. Hydrogen peroxide is an endothelium-derived hyperpolarizing factor in mice. J Clin Invest 2000;106:1521–30.
12. Matoba T, Shimokawa H, Kubota H, et al. Hydrogen peroxide is an endothelium-derived hyperpolarizing factor in human mesenteric arteries. Biochem Biophys Res Comm 2002;290:909–13.
13. Morikawa K, Shimokawa H, Matoba T, et al. Pivotal role of Cu,Zn-superoxide dismutase in endothelium-dependent hyperpolarization. J Clin Invest 2003;112:1871–9.
14. Morikawa K, Fujiki T, Matoba T, et al. Important role of superoxide dismutase in EDHF-mediated responses of human mesenteric arteries. J Cardiovasc Pharmacol 2004;44:552–6.
15. Miura H, Bosnjak JJ, Ning G, Saito T, Miura M, Gutterman DD. Role for hydrogen peroxide in flow-induced dilation of human coronary arterioles. Circ Res 2003;92:e31–40.
16. Yada T, Shimokawa H, Hiramatsu O, et al. Hydrogen peroxide, an endogenous endothelium-derived hyperpolarizing factor, plays an important role in coronary autoregulation in vivo. Circulation 2003; 107:1040–5.
17. Yada T, Shimokawa H, Hiramatsu O, et al. Cardioprotective role of endogenous hydrogen peroxide during ischemia-reperfusion injury in canine coronary microcirculation in vivo. Am J Physiol 2006;291: H1138–46.
18. Jones CJ, DeFily DV, Patterson JL, Chilian WM. Endothelium-dependent relaxation competes with alpha 1- and alpha 2-adrenergic constriction in the canine epicardial coronary microcirculation. Circulation 1993;87:1264–74.
19. Scornik FS, Codina J, Birnbaumer L, Toro L. Modulation of coronary smooth muscle K_{Ca} channels by Gs alpha independent of phosphorylation by protein kinase A. Am J Physiol 1993;265:H1460–5.
20. Tan CM, Xenoyannis S, Feldman RD. Oxidant stress enhances adenylyl cyclase activation. Circ Res 1995;77:710–7.
21. Yada T, Hiramatsu O, Kimura A, et al. In vivo observation of subendocardial microvessels of the beating porcine heart using a needle-probe videomicroscope with a CCD camera. Circ Res 1993; 72:939–46.
22. Mori H, Haruyama Y, Shinozaki H, et al. New nonradioactive microspheres and more sensitive X-ray fluorescence to measure regional blood flow. Am J Physiol 1992;263:H1946–57.
23. Masumoto A, Hirooka Y, Shimokawa H, Hironaga K, Setoguchi S, Takeshita A. Possible involvement of Rho-kinase in the pathogenesis of hypertension in humans. Hypertension 2001;38:1307–10.
24. Matoba T, Shimokawa H, Morikawa K, et al. Electron spin resonance detection of hydrogen peroxide as an endothelium-derived hyperpolarizing factor in porcine coronary microvessels. Arterioscler Thromb Vasc Biol 2003;23:1224–30.
25. Saitoh S, Zhang C, Tune JD, et al. Hydrogen peroxide: a feed-forward dilator that couples myocardial metabolism to coronary blood flow. Arterioscler Thromb Vasc Biol 2006;26:2614–21.
26. Rush JW, Laughlin MH, Woodman CR, Price EM. SOD-1 expression in pig coronary arterioles is increased by exercise training. Am J Physiol 2000;279:H2068–76.
27. Taddei S, Versari D, Cipriano A, et al. Identification of a cytochrome P450 2C9-derived endothelium- derived hyperpolarizing factor in essential hypertensive patients. J Am Coll Cardiol 2006;48:508–15.
28. Duncker DJ, Bache RJ. Regulation of coronary vasomotor tone under normal conditions and during acute myocardial hypoperfusion. Pharmacol Ther 2000;86:87–110.